LBL-38197
UC-800
CONF-9506335--1

Lawrence Berkeley Laboratory
UNIVERSITY OF CALIFORNIA

EARTH SCIENCES DIVISION

Presented at the Second North American Rock Mechanics Symposium, Montreal, Quebec, Canada, June 19–21, 1995, and to be published in the Proceedings

Observations of Joint Persistence and Connectivity Across Boreholes

B.B. Thapa and K. Karasaki

January 1996

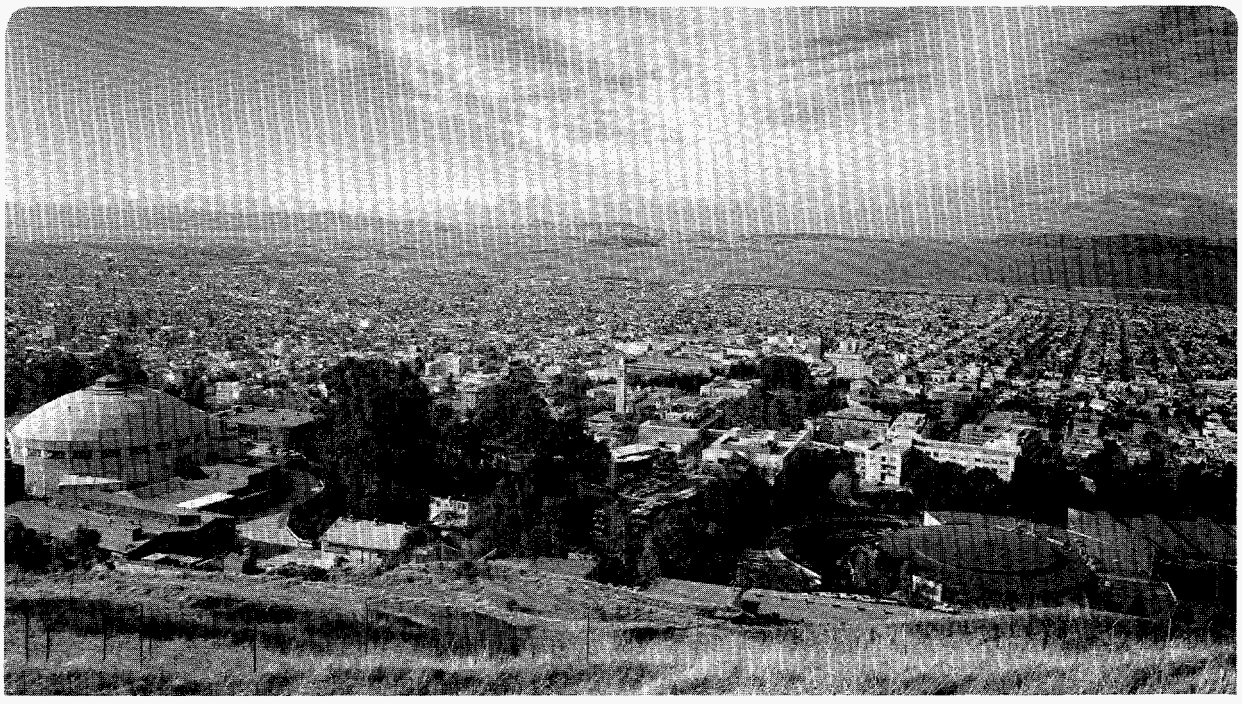

Prepared for the U.S. Department of Energy under Contract Number DE-AC03-76SF00098

LBL-38197
UC-800

Observations of Joint Persistence and Connectivity Across Boreholes

Bhaskar B. Thapa and Kenzi Karasaki

Earth Sciences Division
Ernest Orlando Lawrence Berkeley National Laboratory
University of California
Berkeley, California 94720

January 1996

This work was supported by the Director, Office of Civilian Radioactive Waste Management, Office of External Relations, of the U.S. Department of Energy under Contract No. DE-AC03-76SF00098, and was administered by the Nevada Operations Office, U.S. Department of Energy.

Observations of joint persistence and connectivity across boreholes

Bhaskar B. Thapa
Kenzi Karasaki
Lawrence Berkeley National Laboratory

ABSTRACT: Observations of joint persistence and connectivity are made by comparison of digital borehole wall images of fractures, fluid conductivity logs and hydraulic injections test results. The fractures were found to be generally impersistent across vertical boreholes about 8 m apart. Many hydraulic connections were found in the same volume of rock. Direct connections through single fractures seem to be rare and connectivity appears to be controlled by fracture networks, even over small volumes.

1 INTRODUCTION

Joint persistence and connectivity have strong influences on the hydraulic and mechanical behavior of rockmasses. Interpretation and joint system modeling using estimates of persistence has been described extensively by Dershowitz and Einstein (1988). Persistence and connectivity are difficult to measure however, and often the only way to estimate these parameters is by observation of outcrops or excavation surfaces. In this paper we describe observations of persistence and connectivity made using high resolution digital images of borehole walls combined with fluid conductivity logging (Tsang, 1990) and injection tests.

The borehole wall images were obtained using a relatively new instrument called the Borehole Scanner System (BSS). Conductive fractures were identified using the BSS images and the fluid conductivity results in three boreholes. The orientation, aperture and aperture anisotropies of conductive fractures were extracted from the BSS images. The orientation of the conductive fractures were used to project joint intersections with other boreholes. Since the three borehole studied are fairly close to one another, it was expected that these joints would be persistent enough to make connections across the boreholes and provide direct paths for fluid flow across the boreholes. Similarity of apertures and aperture anisotropies were expected to further enforce the persistency argument on joints with the same orientation that project towards each other based on orientation. These connections in turn were expected to explain the hydraulic pressure response connections between packed of sections of the boreholes observed from the injection test results. This paper describes results made from making these observations at the Lawrence Berkeley Lab's Raymond field site (Karasaki et. al., 1994).

2 THE BOREHOLE SCANNER SYSTEM

The BSS consists of a probe, depth encoder, winch, controller, TV monitor and a VTR unit. The watertight probe houses a white light source and a magnetic compass at the bottom . A mirror rotating at 3000 rpm sits directly above the lamp, and reflects light from the lamp onto the borehole wall through a glass window. The light reflected off the borehole wall directed into a photoelectric transformer. The photoelectric transformer measures the intensity of the incoming light in the red, blue and green wavelength bands and converts the intensities into digital form. The digital data from the photoelectric transformer is passed to an azimuth gauge which marks the point in the data stream corresponding to north. The data then passes through an amplifier to the controller at the surface where it is stored on a digital tape. The entire borehole wall is scanned along a spiral path in this manner as the winch lowers the probe. The maximum vertical resolution is 0.001 mm at present. The resolution along the periphery of the borehole wall depends on the borehole size. An 89 mm diameter borehole will have a horizontal resolution of 0.28 mm. One complete revolution of the probe's mirror picks up reflectance from all of the

contiguous segments on the borehole wall at the same depth. The contiguous segments along the periphery of the borehole wall are discretized into a line of 1000 data points covering reflectance from equal angular intervals. A data point in each such line is a three dimensional vector defining the reflectance intensity, on a scale of 0 to 255, in the red, green and blue (RGB) wavelength bands. The location of the borehole wall segment represented by each such point is defined by the depth at which the point was scanned and the rotation sequence number (1-1000), which specifies the azimuth of the data point with respect to north. Thus the entire borehole wall is represented by lines of RGB data points at successive depths. A true color unrolled image of the borehole wall can be obtained by combining the RGB components of each data point on a computer. Each data point is represented by one pixel on a computer display of the borehole wall. Figure 1 shows a typical image, in monochrome, obtained from BSS data by this process. Thapa (1994) describes the BSS in more detail and compares it to other logging tools.

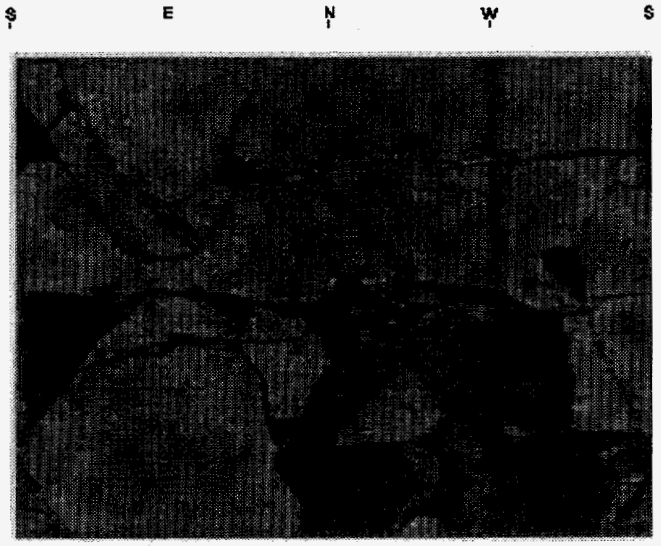

Figure 1: Unrolled image of borehole wall from the BSS

3 BSS SURVEY AT RAYMOND

A number of hydrologic site characterization techniques including the BSS were used at the LBNL site in Raymond California. The Raymond site is situated in the Sierra Nevada foothills about 60 km. south of Yosemite Valley in central California. The general site geology consists of fractured granite overlain by a thin overburden cover. Nine boreholes between 74 to 90 m. in length were drilled at the Raymond site using air-percussion drilling in 1992. Steel casings were placed in the boreholes to a maximum depth of 15 m from ground surface. Figure 2 shows the layout of the boreholes.

The BSS was used to survey the boreholes at Raymond between February and March 1995. Unrolled images of the borehole walls were obtained in five of the Raymond boreholes at a vertical resolution of 0.25 mm and a horizontal resolution of 0.53 mm. Figure 3 shows unrolled images of the entire length of borehole SE1 in a reduced format. Figure 3 provides a useful overall image of subsurface conditions. The locations of discrete features like fractures and dikes are clearly identified by inspection of Figure 3, as are more extensive features like the weathering profile and zones of fracture intersection.

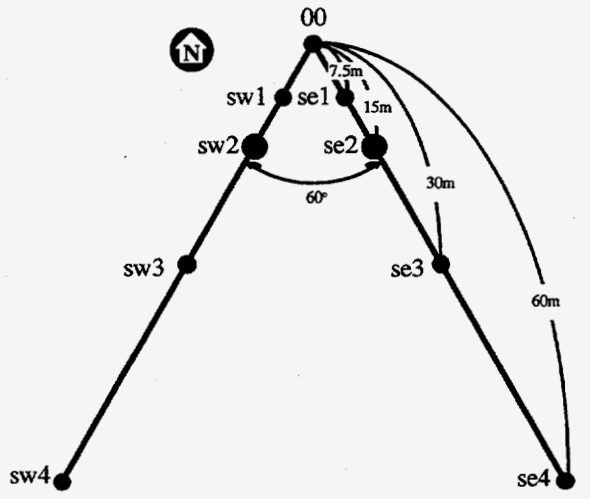

Figure 2: Schematic map of borehole locations at Raymond

Figure 4 shows a more detailed image of the 23-24 m. interval in SE1. The image contains detailed digital data on the lithology and discontinuities in gray scale (all of the actual BSS images are in true color) . Each pixel on the image shown in Figure 4 is defined by reflectance intensities in the red, green and blue wavelength bands as well as a depth recording into the borehole and an azimuth value. This data is amenable to analysis using digital image processing techniques. Thus properties of the fracture seen in the image, such as aperture, may be derived from the BSS data collected at Raymond. In addition to fracture property analysis, the BSS data collected at Raymond made it possible to image fractures in

blow out zones that were not picked up by the alternate approach of using an acoustic televiewer (ATV).

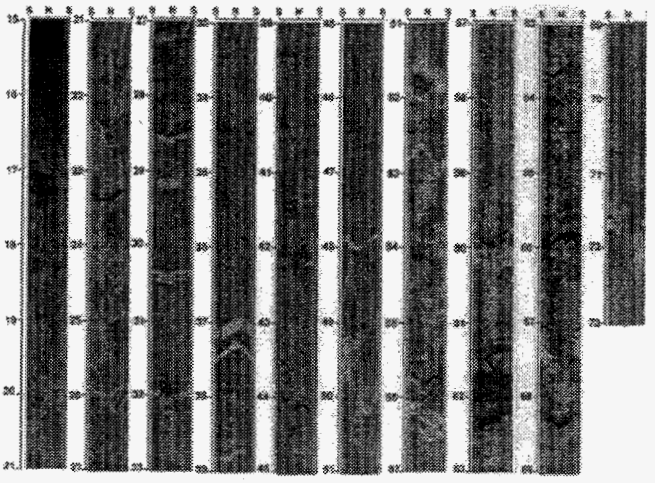

Figure 3: Unrolled image of entire borehole length for SE1

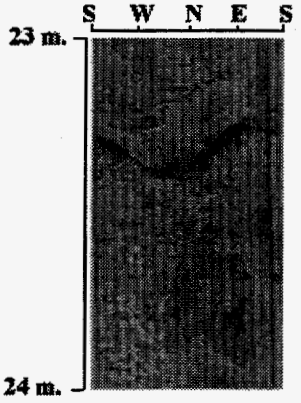

Figure 4: Unrolled image of 23 - 24 m. interval in borehole SE1

4 CONDUCTIVE INTERVAL IDENTIFICATION

Several geophysical surveys and hydrologic tests have been performed at the Raymond site to develop a hydrologic site model. The U.S. Geological Survey logged each of the boreholes at Raymond using the ATV (Paillet et. al., 1985), three-arm caliper, 16 and 64 inch normal resistivity, natural gamma, heat-pulse flowmeter, temperature, single point resistance and spontaneous potential techniques. Cook (1994) inverted injection test results between packed off intervals of injection and response boreholes to obtain an image of hydraulic connectivity between the Raymond boreholes. Cook concludes that there are two inter-borehole connectivity groups: one in the upper east side of the site and the other in the lower west side. The upper group connections dip gently to the north while the lower group connections dip steeply to the south. Cook adds that it is not known whether these groups of connections are manifestations of a network of conductive fractures or just a single fracture. Finally, fluid conductivity logging (Tsang et. al., 1990) was used to identify conductive fractures by logging electrical conductivity in deionized boreholes as the borehole was being pumped. The fluid conductivity logs are used as the primary basis for the identification of conductive fractures in this paper. Figure 6 shows an example of the fluid conductivity log for borehole 00. Figure 5 shows the conductivity recordings with depth on the down scan and the up scan. The down scan is taken to be more accurate since the water ahead of the probe is not disturbed going down the borehole. The sharp peaks in conductivity are indicators of the presence of a flowing fracture.

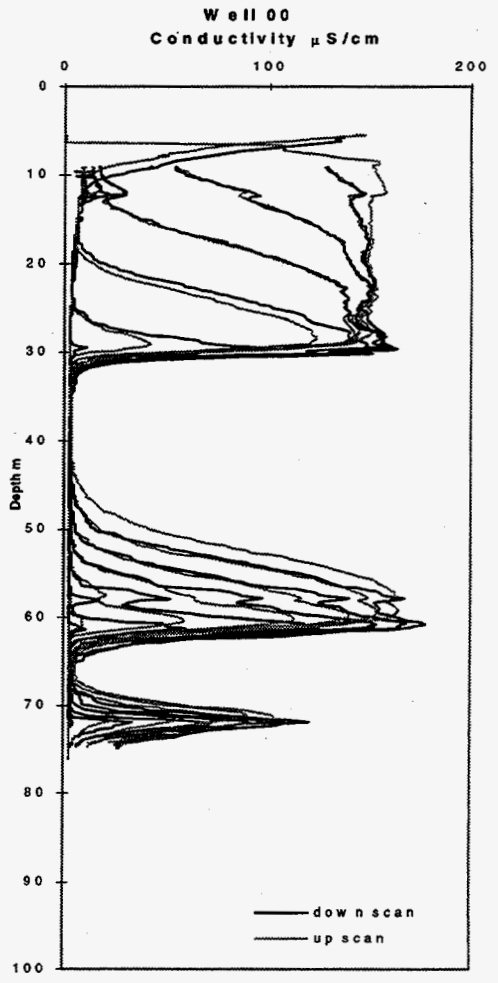

Figure 5: Fluid conductivity log for borehole SE1

5 BSS AND INJECTION TEST RESULTS

Comparison of fluid conductivity logs, like that shown above in Figure 5, with unrolled BSS images led to a number of joints being identified as possibly conductive fractures. In some of the borehole intervals, there was a clearly only one single fracture responsible for the observed conductivity. In other intervals, there were a number of joints and it was not possible to determine a sole conductive fracture. Table 1 summarizes the conductive spots identified from the conductivity logging along with all fractures that could be responsible for the observed conductivity. Table 1 also gives the apertures of the conductive fractures and the orientation based projected intersection depths in other boreholes. The apertures given in Table 1 are estimates of the true aperture. Thapa (1994) describes the method used to obtain these estimates. The aperture anisotropies of the conductive fractures were also obtained for possible use in correlation of fractures across boreholes. Figure 6 shows an example of the aperture anisotropy analysis result.

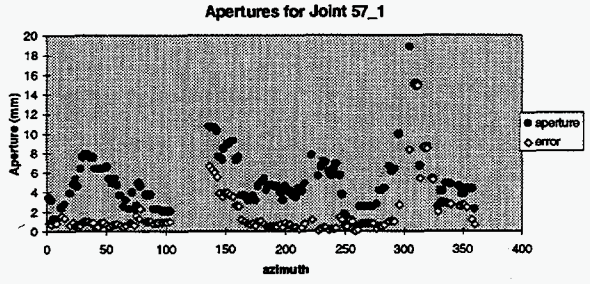

Figure 6: Aperture anisotropy for joint jnt_57_1 of borehole 00

Table 2 shows projected connections between joints in various boreholes. These connections are a subset of the projections shown in Table 1. Only those projections from Table 1 that result in an intersection where a conductive joint exists were taken to be the connections shown in Table 2. In Table 2, the closest conductive joint in the borehole to which a joint was being projected, is shown as being the candidate for the observed connection. Then the candidate connection is further evaluated based on orientation, i.e. only joints with similar orientation in the both origin and observation boreholes are accepted as a persistent connection. Finally the aperture anisotropy of fractures forming persistent connections were compared to further evaluate the likelihood of a persistent joint connection.

Table 1: Conductive joints and orientation based borehole intersection projections

RAYMOND BOREHOLE 00							
Conductive fracture	BSS observation						
by fluid logging	of fractures		orientation	mean	projected	projected	projected
		depth (m)	(dip/dip.dir)	aperture (mm)	00 intercept	se1 intercept	sw1 intercept
1. @29.3 m	1. jnt_29_1	29.22	38/333	16.63	N/A	23.6	27.8
2. @29.9m	2. jnt_29_2	29.65	28/348	27.71	N/A	25.8	27.7
3. @57.9 m	1. jnt_57_0	57.29	56/36	3.88	N/A	51.3	48.1
	2. jnt_57_1	57.34	26/115	4.05	N/A	59.8	55.7
	3. jnt_57_2	57.57	47/163	4.43	N/A	65.3	59.5
	4. jnt_57_3	57.67	17/261	1.98	N/A	57.3	59.4
	5. jnt_57_4	57.87	16/263	1.96	N/A	57.3	59.4
	6. jnt_58_1	58.6	17/259	4.37	N/A	58.2	60.3
4a.@60.4 m	1. jnt_59_1	59.19	36/278	2.74	N/A	56.8	62.5
4b.@61.0 m	2. jnt_59_2	59.32	25/257	5.12	N/A	58.9	62
	3. jnt_59_3	59.4	31/264	4.86	N/A	58.4	62.6
	4. jnt_59_4	59.56	42/195	3.36	N/A	64.9	63.6
	5. jnt_59_5	59.7	51/252	3.57	N/A	59.9	65.6
	6. jnt_59_6	59.9	55/242	4.22	N/A	61.3	68.2
	7. jnt_60_1	60.04	27/283	2.64	N/A	58	62
	8.jnt_60_2	60.19	38/281	2.81	N/A	57.1	63.3
	9. jnt_60_3	60.5	38/26	4.44	N/A	56.7	56.3
	10. jnt_60_4	60.76	43/195	4.57	N/A	66.2	64.8
RAYMOND BOREHOLE SE1							
Conductive fracture	BSS observation						
by fluid logging	of fractures		orientation	mean	projected	projected	projected
		depth (m)	(dip/dip.dir)	aperture (mm)	00 intercept	se1 intercept	sw1 intercept
1. @22.5 m	1. jnt_23_1	23.32	38/329	7.16	28.8	N/A	27.7
	2. jnt_24_1	24.5	66/360	2.39	39.9	N/A	29.1
2. @30.0 m	1.jnt_28_1	28.06	10/235	3.41	27.7	N/A	29
	2.jnt_28_2	28.5	23/9	3.13	31.3	N/A	28.8
	3. jnt_29_0	29.11	39/98	2.53	26.5	N/A	22.6
	4. jnt_29_1	29.4	58/144	3.64	18	N/A	19.3
	5. jnt_29_2	29.64	42/149	3.4	23	N/A	24.5
	6. jnt_29_3	29.83	47/139	3.17	22.4	N/A	22.7
	7. jnt_30_1	30.5	13/5	3.64	32.1	N/A	30.8
3. @31.0 m	1. jnt_30_1	30.5	13/5	3.64	32.1	N/A	30.8
	2. jnt_32_1	32.13	70/145	0.79	12.9	N/A	20
	3. jnt_32_2	32.31	30/29	4.55	35	N/A	30.8
	4. jnt_32_3	32.5	28/60	3.26	33.3	N/A	29.6
	5. jnt_32_4	32.63	18/29	2.83	34.2	N/A	32
RAYMOND BOREHOLE SW1							
Conductive fracture	BSS observation						
by fluid logging	of fractures		orientation	mean	projected	projected	projected
		depth (m)	(dip/dip.dir)	aperture (mm)	00 intercept	se1 intercept	sw1 intercept
1. @14.3 m	1. jnt_14_1	14.3	13/56	3.70	16.1	15.5	N/A
2. @21.5 m	1. jnt_21_1	21.43	20/252	10.51	24	24.1	N/A
3. @64.0m	1. jnt_63_1	63.67	59/173	13.21	70.9	82.5	N/A

Table 2: Connections across boreholes (apertures in mm)

Connection	<——Origin Joint ——>		<——Termination Joint ——>		Orientations	Aperture
Name	Label	Aperture	Label	Aperture	same?	Anisotropy
C1	jnt_29_1 of 00	16.63	jnt_23_1 of SE1	7.16	Y	similar
C2	jnt_29_2 of 00	27.71	jnt_23_1 of SE1	7.16	Y	similar
C3	jnt_59_4 of 00	3.36	jnt_63_1 of SW1	13.21	N	N/A
C4	jnt_60_2 of 00	2.81	jnt_63_1 of SW1	13.21	N	N/A
C5	jnt_60_4 of 00	4.57	jnt_63_1 of SW1	13.21	N	N/A
C6	jnt_23_1 of SE1	7.16	jnt_29_1 of 00	16.63	Y	similar
C7	jnt_28_2 of SE1	3.13	jnt_29_1 of 00	16.63	N	N/A
C8	jnt_29_0 of SE1	2.53	jnt_21_1 of SW1	10.51	N	N/A
C9	jnt_29_3 of SE1	3.17	jnt_21_1 of SW1	10.51	N	N/A
C10	jnt_32_1 of SE1	0.79	jnt_21_1 of SW1	10.51	N	N/A
C11	jnt_21_1 of SW1	10.51	jnt_24_1 of SE1	2.39	N	N/A

Table 3 shows results from the injection test results. Conductive fractures involved in packed off intervals of the injection zone and the response zone are shown for each test. Also, the connection number from Table 2 that explains the observed hydraulic connection is shown in Table 3.

Table 3: Explanation of injection response test results with joint connections

Test 1: Injection into interval 25.4 - 31.3 m of Raymond 00 (includes jnt_29_1, jnt_29_2)											
Response	Zone	Zone	Response	Joints in	Connection	Response	Zone	Zone	Response	Joints in	Connection
Zone - SW1	Top	Bottom	Y/N	Zone	Label	Zone - SE1	Top	Bottom	Y/N	Zone	Label
sw1u	8.65	9.03	0	none	none	se1u	15.6	13.4	0	none	none
sw1um	10.1	23.4	1	jnt_21_1	none	se1um	14.5	34.1	1	all	C1,C2,C6,C7
sw1lm	24.4	37.5	1	none	none	se1lm	35.2	54.9	1	none	none
sw1l	38.6	76.9	1	jnt_63_1	none	se1l	55.9	75.1	1	none	none
Test 2: Injection into interval 56.03 - 61.98 m of Raymond 00 (includes all joints except jnt_29_1, jnt_29_2)											
Response	Zone	Zone	Response	Joints in	Connection	Response	Zone	Zone	Response	Joints in	Connection
Zone - SW1	Top	Bottom	Y/N	Zone	Label	Zone - SE1	Top	Bottom	Y/N	Zone	Label
sw1u	8.65	9.03	0	none	none	se1u	15.6	13.4	0	none	none
sw1um	10.1	23.4	0	jnt_21_1	none	se1um	14.5	34.1	0	all	none
sw1lm	24.4	37.5	0	none	none	se1lm	35.2	54.9	1	none	none
sw1l	38.6	76.9	1	jnt_63_1	C3,C4,C5	se1l	55.9	75.1	1	none	none
Test 3 & 4: Injection into intervals 19.9 - 25.8 m and 25.9 - 31.9 m of Raymond SE1											
(includes 23_1, 24_1 for Test 3 and all joints but 23_1 and 24_1 for Test 4)											
Response	Zone	Zone	Response	Joints in	Connection	Response	Zone	Zone	Response	Joints in	Connection
Zone - SW1	Top	Bottom	Y/N	Zone	Label	Zone - 00	Top	Bottom	Y/N	Zone	Label
sw1u	8.65	9.03	0	none	none	00u	12.2	22.5	1	none	none
sw1um	10.1	23.4	1	jnt_21_1	C8,C9,C10,C11	00um	23.6	30.4	1	29_1, 29_2	C1,C2,C6,C7
sw1lm	24.4	37.5	1	none	none	00lm	31.5	76.2	1	all-	none
sw1l	38.6	76.9	1	jnt_63_1	none	00l	76.2	76.2	0	none	none
Test 5 & 6: Injection into interval 16.1 - 22.1 m and 63.2 - 69.1 m of Raymond SW1											
(includes jnt_14_1, jnt_21_1 for Test 5 and jnt_63_1 for Test 6)											
Response	Zone	Zone	Response	Joints in	Connection	Response	Zone	Zone	Response	Joints in	Connection
Zone - SE1	Top	Bottom	Y/N	Zone	Label	Zone - 00	Top	Bottom	Y/N	Zone	Label
se1u	15.6	13.4	0	none	none	00u	12.2	22.5	1	none	none
se1um	14.5	34.1	1	all	C8,C9,C10,C11	00um	23.6	30.4	1	29_1, 29_2	none
se1lm	35.2	54.9	1	none	none	00lm	31.5	76.2	1	all-	C3,C4,C5
se1l	55.9	75.1	1	none	none	00l	76.2	76.2	0	none	none
all- : all but jnt_29_1, jnt_29_2											

6 DISCUSSION

Within the depth investigated, the conductive fractures form eleven possible direct connections as shown in Table 2. It is unlikely that persistent fractures were missed by this study since all possibly conductive fractures have been analyzed. If the fractures involved in forming these connections were persistent across the boreholes, they would be detected at both ends of the borehole and would provide direct hydraulic connections that would be reflected in the injection test results. In fact, only three of the eleven possible connections actually exist. These three connections (C1, C2 and C6) are formed by jnt_29_1, jnt_29_2 in borehole 00 and jnt_23_1 in borehole SE1. It appears that fracture persistency is correlated to aperture magnitude since all of the conductive fractures have fairly large apertures. However, large apertures do not necessarily imply persistency as seen in the case of jnt_21_1 of borehole SW1 for instance. The aperture anisotropies of the persistent fractures were similar - i.e. they all have relatively larger apertures at about azimuth 75 and 250. From this, it appears that even over small distances (about 8 m.) fractures in granite are generally not persistent.

From Table 3, it can be seen that even if the conductive fractures were persistent only 6 out of 21 positive pressure responses across boreholes could have been explained with single fracture connections. As it is, fractures were mostly impersistent, and only 2 of the 6 single fracture explanations of positive pressure responses actually exist based on the present study. Thus it appears that even over small volumes, the rockmass is well connected by impersistent fractures. This implies that the fracture network, which has not been developed yet for the site, provides the main pathways for fluid flow.

7 CONCLUSIONS

Although it appears that the fractures seen in this study are impersistent, further work is needed to verify that the curvature of these exfoliation fractures are not making them intersect the adjoining borehole at depths different than predicted by plane projections. For connectivity, fracture networks appear to be more important than direct single fracture connections, even over small distances.

Aperture anisotropy provided a useful new method of assessing persistence. The analysis of aperture anisotropy could be expanded to investigate its correlation to fracture surface morphological features using such techniques as described by Bahat (1991).

ACKNOWLEDGMENTS

This work was carried out under U.S. Department of Energy Contract No. DE-AC03 - 76SF00098 for the Director, Office of Civilian Radioactive Waste Management. Office of External Relations, and was administered by the Nevada Operations Office, U.S. Department of Energy. Paul J. Cook provided results from the injection tests.

REFERENCES

Bahat, D. (1991). *Tectonofractography*. Springer-Verlag, Heidelberg.

Cook, P. (1994). *Analysis of interwell hydraulic connectivity in fractured granite*. M.S. Thesis, University of California, Berkeley.

Dershowitz, W.S. and Einstein, H.H. (1988). Characterizing Rock Joint Geometry with Joint System Models. *Rock Mechanics and Rock Engineering*, Vol. 21, pp.21 - 52.

Karasaki, K., Cohen, A., Cook, P., Freifeld, B., Grossenbacher, K., Peterson, J., and Vasco, D. (1994). Hydrologic imaging of fractured rock.

Proc. 18th Int. Symp. on the Scientific Basis for Nuclear Waste Management, Kyoto, Japan.

Paillet, F.L., Keys, W.S., and Hess, A.E. (1985). Effects of lithology on televiewer-log quality and fracture interpretation. *Trans. 26th Annual Logging Symposium*, Society of Professional Well Log Analysts, pp. JJJ1-JJJ31.

Thapa, B.B. (1994). *Analysis of in-situ rock joint strength using digital borehole wall images.* Ph.D. Thesis, University of California, Berkeley

Tsang, C.-F., Hufschmied, P. and Hale, F.V. (1990). Determination of fracture inflow parameters with a borehole fluid conductivity logging method. *Water Resources Research*, Vol.26, No.4, pp.561-578.